ACCEPTED MANUSCRIPT
APL Materials
AIP Publishing
This is the author's peer reviewed, accepted manuscript. However, the online version of record will be different from this version once it has been copyedited and typeset.
PLEASE CITE THIS ARTICLE AS DOI: 10.1063/5.0224193
13 November 2024 11:19:34

1 # Engineering of Co/MgO interface with combination of ultrathin
2 heavy metal insertion and post-oxidation for voltage-controlled
3 magnetic anisotropy effect

4 Hiroyasu Nakayama[1]*, Tomohiro Nozaki[1], Takayuki Nozaki[1], and Shinji Yuasa[1]
5 [1]*National Institute of Advanced Industrial Science and Technology, Research Center for*
6 *Emerging Computing Technologies, Tsukuba, Ibaraki 305-8568, Japan*
7
8 *Authors to whom correspondence should be addressed: nakayama.hiroyasu@aist.go.jp
9
10
11 **ABSTRACT**
12 The voltage-controlled magnetic anisotropy (VCMA) effect in
13 ferromagnet/insulator junctions provides an effective way to manipulate electron
14 spins, which can form the basis of future magnetic memory technologies. Recent
15 studies have revealed that the VCMA effect can be strongly tuned by a process of
16 'interface engineering' exploiting ultrathin heavy metal layers and an electron
17 depletion effect. To further decrease the numbers of electrons, chemical reactions
18 such as surface oxidation of ferromagnets may also be an effective way to achieve
19 this depletion. However, the knowledge of combined effect of heavy metal layers
20 and oxidation is still lacking. Here, we demonstrate that dual interfacial
21 engineering using an insertion of heavy metals (Pt or Re) and a post-oxidation
22 process can have a remarkable effect on the perpendicular magnetic anisotropy and
23 the VCMA effect. Interestingly, a strong enhancement of the perpendicular
24 magnetic anisotropy is observed by dual interfacial engineering with Pt insertion,
25 whereas it does not occur with Pt insertion or surface oxidation alone. Furthermore,
26 even a sign reversal of the additional VCMA effect due to the ultrathin heavy metal
27 layers is observed by utilizing dual interfacial engineering. These findings provide
28 another degree of freedom for designing voltage-controlled spintronic devices and
29 pave the way to interfacial spin-orbit engineering for the VCMA effect.
30
31
32

33 ## I. INTRODUCTION

34 Recently, spin manipulation making use of the interface with broken inversion 35 symmetry is attracting much attention in the rapidly evolving field of spin-orbitronics.[1] Since 36 it enables spin manipulation with a low power consumption, the use of the voltage-controlled 37 magnetic anisotropy (VCMA) effect at the interface of a ferromagnet/non-magnetic insulator 38 is a promising technology toward future spintronic devices.[2–4] The VCMA effect is an 39 interfacial phenomenon that drives the change of the magnetic anisotropy of the ferromagnet 40 by applying an external voltage through the adjacent insulator (see Fig. 1). Moreover, the 41 purely electronic VCMA effect, free from chemical reactions and the displacement of ions,[5] 42 enables spin manipulation with high-speed response and high writing endurance,[6,7] which 43 can be of considerable benefit for practical spintronic devices. For the mechanism of the 44 purely electronic VCMA effect at ferromagnet/insulator junctions, contributions such as the 45 voltage-modulation of the band structure, the electron occupation state,[8–10] the Rashba spin-46 orbit anisotropy,[11] and the magnetic dipole moment[12] have been proposed.

47 To operate voltage-controlled spintronics devices based on the VCMA effect with 48 lower power consumption, materials exhibiting a large VCMA coefficient are desirable. The 49 VCMA coefficient is defined by $\Delta K_{\mathrm{PMA}} t/E$, where ΔK_{PMA} is the change of the effective 50 perpendicular magnetic anisotropy (PMA) energy induced by the applied electric field, t is 51 the thickness of the ferromagnetic layer, and E is the applied electric field given by $V_{\mathrm{bias}}/t_{\mathrm{barrier}}$. 52 Here, V_{bias} and t_{barrier} are the applied bias voltage and the thickness of the tunneling barrier, 53 respectively. A positive bias voltage induces electron accumulation at the ferromagnetic 54 layer/insulator layer interfaces as shown in Fig. 1. A negative (positive) VCMA coefficient 55 describes a reduction (enhancement) of the PMA with applying the positive bias voltage. 56 Therefore, at the ferromagnetic layer/insulator layer interfaces with negative (positive) 57 VCMA effect, the PMA decreases (increases) due to electron accumulation.

58 Since the VCMA effect is an interfacial phenomenon, it can be strongly tuned by 59 interfacial engineering. One method involves the insertion of a sub-atomic layer of heavy 60 metals at the interface between the ferromagnet and an insulator. In a previous study, the 61 effect of inserting a layer of 4*d* and 5*d* transition metals at Fe/MgO junction has been 62 theoretically calculated via the first principles calculations.[13] The results suggest that the 63 magnitude of the spin-orbit coupling of the inserted materials and the position of the Fermi 64 level with respect to the *d*-band level can be important factors to tune the VCMA effect. Thus, 65 5*d* transition metals such as Pt and Ir are promising materials for the insertion layer because 66 they exhibit large spin-orbit interactions and magnetic proximity effects. This concept has

AIP Publishing APL Materials ACCEPTED MANUSCRIPT
This is the author's peer reviewed, accepted manuscript. However, the online version of record will be different from this version once it has been copyedited and typeset.
PLEASE CITE THIS ARTICLE AS DOI: 10.1063/5.0224173
13 November 2024 11:19:34

67 been demonstrated in epitaxially grown Fe/MgO based junctions with Ir doping.[14,15] In our
68 recent experimental studies on interface engineered Co/MgO junctions, we have
69 demonstrated a strong enhancement of the negative VCMA effect by inserting a sub-atomic
70 layer of Pt.[16,17]

71 Another method to tune the VCMA effect via interfacial engineering is to control
72 the oxidation state at the interface between the ferromagnetic material and the insulator.
73 Although it is known that the sign of the VCMA effect is negative in most materials, a
74 positive VCMA effect can be observed by exploiting an interface between surface oxidized
75 Co and high-*k* materials such as HfO_2[18] and TiO_x.[19,20] Interestingly, a large positive VCMA
76 coefficient up to +230 fJ/Vm can be obtained for Co/CoO_x/HfO_2 junctions. A positive
77 VCMA effect has also been detected for ultrathin-Co/MgO/HfO_2[21] and Ru/CoFeB/MgO[22]
78 structures with MgO barriers deposited by sputtering. However, for the case of a sputter-
79 deposited MgO barrier, it has been pointed out that the sign reversal of the VCMA effect can
80 occur due to a slight change in the oxidation state at the junction interface.[23] By controlling
81 the oxidation state at the interface by inserting the light metal MgAl, a large VCMA
82 coefficient and a large PMA have been demonstrated in epitaxially grown single crystalline
83 Fe/MgO based structures deposited by molecular beam epitaxy.[24] Although a lot of efforts
84 are made to elucidate the physical mechanism of the VCMA effect so far, the effect of
85 interfacial engineering including both interfacial oxidation and the insertion of sub-atomic
86 layer of heavy metals remains to be thoroughly investigated.

87 In this study, we report on the impact of dual interfacial engineering utilizing heavy
88 metal insertion and post-oxidation process on the PMA and the VCMA effect of Co/MgO
89 based junctions. We used Pt and Re for the materials of insertion layers since Pt (Re) shows
90 electron doping (depletion) for the adjacent Co layer, and thus systematic changes of the
91 VCMA effect due to the insertion of this layer may be expected. We found that the PMA of
92 the Co/MgO junction is enhanced (reduced) by conducting an oxidation process for the films
93 with sub-atomic layer of Pt (Re) inserted, which is quite different from the case simply
94 inserting heavy metal elements.[16,17] Moreover, the signs of the additional VCMA coefficient
95 due to the insertion of the sub-atomic layer of heavy metals are reversed by conducting an
96 oxidation process after heavy metal insertion, interestingly. These results suggest the crucial
97 role of heavy metals on the magnetic anisotropy for both unoxidized Co/MgO junctions and
98 surface oxidized Co/MgO junctions. These findings will provide crucial information towards
99 further development of the interfacial spin-orbit engineering for control of the VCMA effect.
100

ACCEPTED MANUSCRIPT
APL Materials
AIP Publishing
This is the author's peer reviewed, accepted manuscript. However, the online version of record will be different from this version once it has been copyedited and typeset.
PLEASE CITE THIS ARTICLE AS DOI: 10.1063/5.0224153
13 November 2024 11:19:34

AIP Publishing
APL Materials
ACCEPTED MANUSCRIPT
This is the author's peer reviewed, accepted manuscript. However, the online version of record will be different from this version once it has been copyedited and typeset.
PLEASE CITE THIS ARTICLE AS DOI: 10.1063/5.0224173
13 November 2024 11:19:34

II. EXPERIMENTAL DETAILS

A. Sample preparation

The sample system used for the VCMA measurements consists of Ta(5 nm)/Ru(10 nm)/Ta(5 nm)/Pt(2 nm)/Ru(4 nm)/Co(0.7-1.5 nm)/*X* (*X*=Pt or Re)(0-0.28 nm)/oxidation process/MgO(3 nm)/ITO(20 nm) polycrystalline film deposited on thermally oxidized silicon substrate, where the order of the layers is described from bottom to top. For the control measurements, we also prepared the multilayer films without *X* layers and/or oxidation process. The deposition of the multilayer film was performed at room temperature by a combination of sputtering and molecular beam epitaxy apparatuses without breaking the vacuum. Most layers were deposited by magnetron sputtering, and only the MgO layers were formed by electron-beam evaporation. To evaluate the PMA and the VCMA effect by using a polar-MOKE apparatus with a perpendicular magnetic field, we utilized Ru as underlayers. Although a large change of the VCMA coefficient with inserting *X* layer has reported for Co/*X*/MgO junctions with Os underlayer,[17] Os is known to be toxic when oxidized. Therefore, in the present study, we used Ru as the alternative of Os because Ru is expected to show similar structural and electrical properties as Os. The layer of heavy metal *X* and the oxidation process were introduced to change the magnitude of the PMA and the VCMA effect. The thicknesses of Co, t_{Co}, and *X*, t_X, were varied by using a linear shutter. The oxidation process in an oxygen atmosphere was conducted using pure oxygen gas at a pressure of 0.5 Pa for 3 minutes in an oxidation chamber directly connected to the sputtering apparatus. For the top electrode, transparent ITO (indium tin oxide) was used for evaluating the magnetic properties of the ultrathin Co layer using polar-MOKE. To prevent heavy metals from diffusing into the Co layer, no annealing was done for any of the multilayer films. The VCMA devices were fabricated by conventional optical lithography, ion-milling, and lift-off processes. The cross-sectional area of the tunnel junction was 8×10 μm^2.

B. Measurements of magnetic properties

The magnetic properties of the multilayer films were evaluated by a combination of VSM and polar-MOKE. For the VSM measurements, multilayer films of Ta(5 nm)/Ru(10 nm)/Ta(5 nm)/Pt(2 nm)/Ru(4 nm)/Co(0.94-1.58 nm)/MgO(3 nm)/ITO(20), Ta(5 nm)/Ru(10 nm)/Ta(5 nm)/Pt(2 nm)/Ru(4 nm)/Co(1.1-1.74 nm)/oxidation process/MgO(3 nm)/ITO(20), and Ta(5 nm)/Ru(10 nm)/Ta(5 nm)/Pt(2 nm)/Ru(4 nm)/Co(1.26-1.58 nm)/*X* (*X*=Pt or Re)(0.03 nm)/oxidation process/MgO(3 nm)/ITO(20) were used. For the polar-MOKE

measurements, a semiconductor laser with a spot size of 1.5 μm was utilized, which was much smaller than the cross-sectional area of the tunnel junctions. The change in the Kerr rotation angle was measured by applying an external magnetic field perpendicular to the film plane. For the VCMA measurements, polar-MOKE apparatus equipped with a micro-probe system was utilized. All the measurements were conducted at room temperature.

III. RESULTS AND DISCUSSION

A. Influence of post-oxidization on magnetic properties of Co/MgO based junctions

To investigate the effect of the oxidation process on the values of the saturation magnetization M_S and the thickness of the magnetic dead layer t_{dead} of the Co layer, we first carried out vibrating sample magnetometry (VSM) measurements. Here, the oxidation process was performed using pure oxygen gas at a pressure of 0.5 Pa for 3 minutes for Co surfaces [also see Fig. 2(a) and experimental details]. In Fig. 2(b), the saturation magnetic moment per unit area for the Co/MgO films with and without interfacial engineering due to the oxidation process is plotted as a function of the nominal Co layer thickness t_{Co}. The results shows that the saturation magnetic moment per unit area increases linearly with increasing t_{Co} for both with and without the oxidation process. Here, the linear fit to the data shown by the dashed line gives the values of M_S and t_{dead}, i.e., the values obtained from the slope and the intercept with the horizontal axis are M_S=1417 kAm^{-1} and t_{dead}=0.12 nm for the films without the oxidation process. The magnitude of M_S obtained for films without the oxidation process is close to the value of the similar Co/MgO films grown on Pt or Os underlayers reported in previous works,[16,17] indicating a similar quality of the Co/MgO films on the Ru underlayer. The obtained t_{dead} is also almost consistent with the Co/MgO films with an Os underlayer. On the other hand, the magnitudes of M_S and t_{dead} obtained for the films with oxidation process are M_S=1344 kAm^{-1} and t_{dead}=0.66 nm, respectively. These values are closer to those reported for the films with an oxidation process using TiO_x layers.[19] The increase of the dead layer due to the oxidation process, which corresponds to the thickness of 0.54 nm, can be mainly due to the oxidation of the Co layer. With similar oxidation conditions, it was demonstrated that CoO_x is mainly dominated by CoO in previous studies.[25,26] Therefore, here we assumed CoO_x as CoO. Considering the lattice parameters of Co and CoO as 2.51 and 4.23 Å, respectively,[19] the increase of the insulator layer thickness due to the oxidation can be calculated as 0.91 nm. Thus, we evaluated the PMA and the VCMA effect by considering the increases of the dead layer and the insulator layer

AIP Publishing APL Materials ACCEPTED MANUSCRIPT
This is the author's peer reviewed, accepted manuscript. However, the online version of record will be different from this version once it has been copyedited and typeset.
PLEASE CITE THIS ARTICLE AS DOI: 10.1063/5.0224123
13 November 2024 11:19:34

169 thicknesses due to the oxidation process. Compared with the unoxidized films, the slight
170 decrease with M_S may be due to the non-uniformity of the oxidation level. It should be noted
171 here that only a small difference was observed in the saturation magnetic moment per unit
172 area in the multilayer films after inserting a sub-atomic layer of heavy metal X (=Pt or Re)
173 followed by the oxidation process [see Fig. 2(b)], suggesting that the oxidation state of Co
174 cannot be controlled by inserting sub-atomic layer of X. Here, the orange and the green plots
175 are the data with insertion of X=Pt and Re, respectively. The thickness of X, t_X, was fixed at
176 0.03 nm to evaluate the PMA and the VCMA effect using a polar magneto-optical Kerr effect
177 (polar-MOKE) apparatus with a perpendicular magnetic field, which will be discussed later.
178 For the samples without the oxidation process, in addition, it is known that almost no
179 difference was observed in the saturation magnetic moment per unit area in the multilayer
180 films with inserting a sub-atomic layer of heavy metals.[16] Thus, hereafter, the values of M_S
181 and t_{dead} for Co/MgO given above for each condition are used to determine the values of the
182 PMA and the VCMA coefficient in the multilayer films with the insertion of heavy metal
183 layers.
184

185 **B. Perpendicular magnetic anisotropy**

186 Next, we conducted polar-MOKE measurements to quantitatively evaluate the
187 PMA for both films with and without the oxidation process. To clarify the effect of insertion
188 of heavy metal X layer and the surface oxidation, we measured the X thickness t_X dependence
189 of the polar-MOKE hysteresis curves. In Figs. 3(a)-(d), the perpendicular magnetic field
190 H_{perp} dependence of the Kerr rotation angle for different X and thicknesses t_X are shown,
191 where the effective thickness of the Co layer t_{Co}* (=t_{Co}−t_{dead}) is fixed at 0.8 nm. Due to the
192 multilayer films with an in-plane magnetic easy axis, a gradual switching is obtained for
193 Co/MgO junctions, where X is not inserted. The magnitude of the saturation magnetic field
194 decreases with increasing X thickness, reflecting an enhancement of the PMA at the Co/MgO
195 interface. For the films with the insertion of Re without the oxidation process [see Fig. 3(b)],
196 the saturation magnetic field slightly increases with increasing X thickness when t_X>0.08 nm,
197 which may be caused by the deterioration of film quality caused by the sputtering of heavy
198 metal Re. Therefore, we only utilized the devices with t_X<0.08 nm for the VCMA
199 measurements. For the case with the insertion of Pt layer with the oxidation process [see Fig.
200 3(c)], a sharp switching due to the out-of-plane magnetic easy axis is obtained when t_{Pt} is
201 only 0.08 nm, indicating a strong enhancement of the PMA.
202 Since the Kerr rotation angle obtained by the polar-MOKE measurements is

ACCEPTED MANUSCRIPT
APL Materials
AIP Publishing
This is the author's peer reviewed, accepted manuscript. However, the online version of record will be different from this version once it has been copyedited and typeset.
PLEASE CITE THIS ARTICLE AS DOI: 10.1063/5.0224173
13 November 2024 11:19:34

203 proportional to the perpendicular magnetization component of the ferromagnetic Co layer,
204 M_{perp}, the effective PMA energy K_{PMA} of the Co layer can be evaluated from the $M_{\mathrm{perp}}(H_{\mathrm{perp}})$
205 area combined with the values of saturation magnetization M_S determined by the VSM
206 measurements. Here, K_{PMA} can be evaluated by using following equation:[27]

207 $$K_{\mathrm{PMA}} = \frac{\mu_0}{2}\int_{-M_S}^{M_S} \left|H_{\mathrm{perp}}\right| dM \quad (1)$$

208 where μ_0 is the magnetic permeability of vacuum. Figs 4(a)-(d) shows the X thickness
209 dependence of $K_{\mathrm{PMA}}t_{\mathrm{Co}}$* for multilayer films with the insertion of X. In Figs 4(a) and 4(b),
210 the magnitude of the change in $K_{\mathrm{PMA}}t_{\mathrm{Co}}$* due to the insertion of the heavy metal layer without
211 oxidation process increases with increasing the thickness of X and is similar to the case of
212 Co/MgO junctions with Pt or Os underlayers.[16,17] For the films with the oxidation process as
213 shown in Figs. 4(c) and 4(d), interestingly, the magnitude of the change in $K_{\mathrm{PMA}}t_{\mathrm{Co}}$* due to
214 the insertion of the heavy metal layer is significantly enhanced when compared with
215 unoxidized Co/MgO junctions. Particularly for the films with Pt insertion, a larger difference
216 was observed for the films with and without the oxidation process. Focusing on the films
217 with t_{Co}*≈0.8 nm and t_X=0 nm in Figs. 4(a)-(d), the magnitude of $K_{\mathrm{PMA}}t_{\mathrm{Co}}$* decrease after
218 conducting the oxidation process suggests that the insertion of an X layer is necessary to
219 obtain a greater enhancement of the PMA energy by means of interfacial engineering.
220 However, for the films with Re insertion [also see the data of t_{Co}*≈0.8 nm in Figs. 4(a)-(d)],
221 the magnitude of $K_{\mathrm{PMA}}t_{\mathrm{Co}}$* decrease after conducting oxidation implies that the selection of
222 an appropriate material for X is also necessary.
223

224 **C. Voltage-controlled magnetic anisotropy effect**

225 Here, we show the effect of inserting a heavy metal layer on the VCMA effect.
226 Focusing on films without an oxidation process, the typical polar-MOKE hysteresis curves
227 of Co/MgO junctions without heavy metal layers inserted are shown in Fig. 5(a) and the case
228 with heavy metal layers inserted are shown in Figs. 5(b) and 5(c), where the effective
229 thickness of Co layer is fixed at 0.8 nm. To show the differences in the effect of the insertion
230 layer, here, the thickness of the inserted Pt and Re layers are set to 0.03 and 0.01 nm,
231 respectively. To measure the VCMA effect, we applied a DC bias voltage through the MgO
232 barriers for these multilayer devices. In Figs. 5(a)-(c), the red and blue data were measured
233 under application of V_{bias}=+0.8 and −0.8 V, respectively. The inset shows a magnified view
234 of the main curves and reveals that clear shifts in the saturation field due to the V_{bias} are
235 obtained in all the cases, indicating the occurrence of a VCMA effect. Here, the K_{PMA} of the
236 ferromagnetic layer can be determined in the same manner as in the case of Figs. 4(a)-(d) by

AIP Publishing APL Materials ACCEPTED MANUSCRIPT
This is the author's peer reviewed, accepted manuscript. However, the online version of record will be different from this version once it has been copyedited and typeset.
PLEASE CITE THIS ARTICLE AS DOI: 10.1063/5.0224133
13 November 2024 11:19:34

237 using Eq. (1). Since the change of the Kerr rotation angle due to the bias voltage was
238 negligibly small when enough large H_{perp} was applied, we assumed that the M_S is not changed
239 by applying bias voltage. The magnitude of the $K_{PMA}t_{Co}$* values obtained for each bias
240 voltage condition are summarized in Figs. 5(d)-(f), respectively. Here, linear changes in
241 $K_{PMA}t_{Co}$* are obtained for all the samples and the magnitude of the slope corresponds to the
242 VCMA coefficient. Considering the thickness of the insulator layer [MgO(3 nm)], the
243 VCMA coefficient of Co/MgO junctions without the insertion layer and with Pt and Re
244 insertion layers are determined as −37, −80, and −23 fJ$V^{-1}m^{-1}$, respectively. These results
245 indicate that the sign of the additional VCMA effect induced by inserting X is negative
246 (positive) for Pt (Re), which is same as the case of inserting Pt (Os) for the Co/MgO junctions
247 deposited on Pt and Os underlayers.[16,17] Since Pt (Re and Os) exhibits electron doping
248 (depletion) for the adjacent Co layer, charge transfer between X and Co layers may affect the
249 magnitude of the VCMA effect. The values of the additional VCMA coefficient induced by
250 X insertion $\Delta\xi$ are maintained over the range of the inserted layer used in this study [see Fig.
251 7(a)]. Since the sign of the VCMA effect in most materials is negative, here, the negative
252 values are placed at the top of the vertical axis in Fig. 7.

253 Now, let us show the impact of the oxidation process in addition to the insertion of
254 a sub-atomic layer of heavy metals. In a similar process as the case of the films without the
255 oxidation process, the typical polar-MOKE hysteresis curves of Co/MgO junctions without
256 heavy metal layers inserted are shown in Fig. 6(a) and the case with heavy metal layers
257 inserted are shown in Figs. 6(b) and 6(c), where the effective thickness of the Co layers is
258 fixed at 0.8 nm. Here, the thickness of the inserted X layers is set to 0.02 nm to show the
259 differences in the effect of the insertion layers. The magnitude of the $K_{PMA}t_{Co}$* obtained for
260 each V_{bias} are summarized in Figs. 6(d)-(f), respectively. Here, linear changes in $K_{PMA}t_{Co}$*
261 are again obtained for all the samples. However, a positive VCMA effect is obtained for the
262 films without X insertion and with Pt insertion as shown in Figs. 6(d) and 6(e). These results
263 are quite different from the case of the films with unoxidized Co/MgO junctions, suggesting
264 the impact of surface oxidation of Co on the VCMA effect. Since the effective thicknesses
265 of Co layers t_{Co}* in the films with and without oxidation shown in Figs. 5 and 6 are the same,
266 we cannot explain the sign reversal simply by a decrease in the effective thickness due to the
267 oxidation process. By considering the thickness of the insulator layers [CoO_x(0.91
268 nm)/MgO(3 nm)], the VCMA coefficient of Co/MgO junctions without the insertion layer
269 and with Pt and Re insertion layers are determined as +3, +13, and −8 fJ$V^{-1}m^{-1}$, respectively.
270 Interestingly, the signs of the additional VCMA coefficient induced by X insertion are

AIP Publishing APL Materials ACCEPTED MANUSCRIPT
This is the author's peer reviewed, accepted manuscript. However, the online version of record will be different from this version once it has been copyedited and typeset.
PLEASE CITE THIS ARTICLE AS DOI: 10.1063/5.0224173
13 November 2024 11:19:34

271 reversed by conducting the oxidation process (see Fig. 7). Although further research is
272 necessary, these results may imply the existence of a mechanism such as the voltage-induced
273 atomic structural change[28] for the additional VCMA effect induced by X insertion in
274 Co/MgO based junctions with surface oxidation.

275 Here, we conducted control experiments to further explore the origin of the
276 modulation of the VCMA effect via dual interfacial engineering. As a control measurement,
277 firstly, we changed the oxidation conditions. While the oxidation level was fixed to one
278 condition in the above experiments, we also investigated the VCMA effect using a similar
279 sample structure but using a different oxidation condition [also see Fig. S3(c) in Section S1,
280 supplementary material]. By utilizing films with a weaker oxidation level, a negative VCMA
281 effect is observed without the Pt insertion layer. On the other hand, the sign of the additional
282 VCMA coefficient $\Delta\xi$ due to the insertion of a sub-atomic layer of Pt is positive, which is
283 similar to the results in Fig. 7(b). These results suggest that the oxidation level strongly
284 influences the magnitude of the VCMA effect, whilst the magnitude of the additional VCMA
285 coefficient due to the insertion of X, $\Delta\xi$, is maintained relatively constant even when the
286 oxidation level changes. In another control experiment, we changed the order of the heavy
287 metal insertion and the interfacial oxidation. Although the oxidation process was performed
288 after the insertion of heavy metal layers in the above experiments, we also investigated the
289 VCMA effect using a film in which the heavy metal insertion was conducted after interfacial
290 oxidation of the Co layer [also see Fig. S4(d) in Section S2, supplementary material]. In this
291 case, almost no change is observed in the additional VCMA coefficient due to the insertion
292 of a sub-atomic layer of Pt. Here, a change of the PMA energy due to the insertion of the Pt
293 layer is not observed as well [see Fig. S4(c) in Section S2, supplementary material].
294 Therefore, a direct contact or alloying between the ferromagnetic metal Co and the heavy
295 metal may be necessary to achieve an enhancement of the PMA and a sign reversal for the
296 additional VCMA coefficient by using the dual interfacial engineering.

297 Finally, we discuss the prospect of dual interfacial engineering using the insertion
298 of a sub-atomic layer of heavy metals and an oxidation process for voltage-controlled
299 phenomena in terms of the technical aspects. Although we have only utilized Ru as the
300 underlayer and sub-atomic Pt and Re as the insertion layer in this study, the influence of
301 underlayer materials on the VCMA effect at interface engineered Co/MgO junctions with
302 heavy metals has been reported elsewhere.[17] The magnitude of the modulated PMA and
303 VCMA via the dual interfacial engineering method might be further enhanced by using other
304 materials as the underlayer and/or the insertion layer, and by using different thickness

ACCEPTED MANUSCRIPT
APL Materials
AIP Publishing
This is the author's peer reviewed, accepted manuscript. However, the online version of record will be different from this version once it has been copyedited and typeset.
PLEASE CITE THIS ARTICLE AS DOI: 10.1063/5.0224173
13 November 2024 11:19:34

305 insertion layer to control the oxidation state of Co. Thus, further research is still necessary
306 to clarify the correlation between the PMA, VCMA effect, interfacial oxidation state, and
307 underlayer materials. While we have focused on experiments at room temperature in this
308 study, CoO_x layers formed by naturally oxidized Co are known to exhibit anti-
309 ferromagnetism below 200 K, and thus, an exchange bias can be observed for Co/CoO_x
310 junctions at lower temperature.[29] By exploiting the dual interfacial engineering reported in
311 this study, a modulation of the Neel temperature, the magnitude of the exchange bias, and
312 their voltage-controlled efficiencies may be expected. Recent studies revealed that the
313 exchange bias can be modulated by the spin-orbit torque.[30–32] Therefore, more efficient spin
314 manipulation may be expected by utilizing dual interfacial engineering, exchange bias, and
315 the combination of spin-orbit torque and voltage-controlled magnetic properties.
316
317
318 **IV. CONCLUSION**
319 In summary, we have experimentally demonstrated dual interfacial engineering
320 exploiting the insertion of sub-atomic 5*d* transition metals (Pt or Re) and post-oxidation
321 process on the PMA and the VCMA effect of Co/MgO based junctions. We found that the
322 PMA of Co/MgO junction is strongly enhanced by introducing an ultrathin heavy metal Pt
323 layer, followed by a post-oxidation process, which is quite different from the case merely
324 inserting heavy metal Pt without an oxidation process.[16,17] Furthermore, the additional
325 VCMA coefficient due to the insertion of the sub-atomic layer of heavy metals intriguingly
326 shows sign reversal when introducing an oxidation process after the heavy metal insertion.
327 Thus, our findings will offer another pathway for designing voltage-controlled spin-
328 orbitronic devices based on the VCMA effect.
329
330
331 **SUPPLEMENTARY MATERIAL**
332 See the supplementary material for the magnetic properties and VCMA effect of multilayer
333 films with post oxidation in air atmosphere, and magnetic properties and VCMA effect of
334 multilayer films with *X* insertion after oxidation process.
335
336
337 **ACKNOWLEDGMENTS**
338 The authors thank T. Yamamoto, T. Ichinose, H. Onoda, and Y. Hibino of the National

APL Materials ACCEPTED MANUSCRIPT
AIP Publishing
This is the author's peer reviewed, accepted manuscript. However, the online version of record will be different from this version once it has been copyedited and typeset.
PLEASE CITE THIS ARTICLE AS DOI: 10.1063/5.0224173
13 November 2024 11:19:34

ACCEPTED MANUSCRIPT
APL Materials
AIP Publishing
This is the author's peer reviewed, accepted manuscript. However, the online version of record will be different from this version once it has been copyedited and typeset.
PLEASE CITE THIS ARTICLE AS DOI: 10.1063/5.0224193
13 November 2024 11:19:34

339 Institute of Advanced Industrial Science and Technology, H. Sukegawa and S. Mitani of the
340 National Institute for Materials Science, and Y. Kageyama, L. Sakai, K. Hiraga, K. Ohba, Y.
341 Higo, and M. Hosomi of Sony Semiconductor Solutions Corporation for their fruitful
342 discussions. This work was partially supported by the Japan Science and Technology Agency
343 (JST), PRESTO Grant Number JPMJPR23H6, Japan and the New Energy and Industrial
344 Technology Development Organization (NEDO) Grant Number JPNP16007, Japan.

345

346

347 **AUTHOR DECLARATIONS**

348 **Conflict of Interest**

349 The authors have no conflicts to disclose.

350

351 **Author Contributions**

352 **Hiroyasu Nakayama**: Conceptualization (lead); Data curation (lead); Formal analysis
353 (lead); Funding acquisition (equal); Investigation (lead); Methodology (lead); Writing –
354 original draft (lead); Writing – review & editing (lead).

355 **Tomohiro Nozaki**: Data curation (supporting); Formal analysis (supporting); Investigation
356 (supporting); Methodology (supporting); Writing – review & editing (supporting).

357 **Takayuki Nozaki**: Data curation (supporting); Formal analysis (supporting); Investigation
358 (supporting); Methodology (supporting); Writing – review & editing (supporting).

359 **Shinji Yuasa**: Funding acquisition (lead); Investigation (supporting); Project administration
360 (equal); Writing – review & editing (supporting).

361

362

363 **DATA AVAILABILITY**

364 The data that support the finding of this study are available from the corresponding author
365 upon reasonable request.

366

367 **REFERENCES**

368 [1] F. Trier, P. Noël, J. Von Kim, J.P. Attané, L. Vila, and M. Bibes, Nat. Rev. Mater. **7**, 258
369 (2022).
370 [2] T. Nozaki, T. Yamamoto, S. Miwa, M. Tsujikawa, M. Shirai, S. Yuasa, and Y. Suzuki,
371 Micromachines **10**, 327 (2019).
372 [3] S. Miwa, M. Suzuki, M. Tsujikawa, T. Nozaki, T. Nakamura, M. Shirai, S. Yuasa, and Y.
373 Suzuki, J. Phys. D. Appl. Phys. **52**, 063001 (2019).
374 [4] Y. Shao and P.K. Amiri, Adv. Mater. Technol. **8**, 2300676 (2023).
375 [5] U. Bauer, L. Yao, A.J. Tan, P. Agrawal, S. Emori, H.L. Tuller, S. van Dijken, and G.S.D.
376 Beach, Nat. Mater. **14**, 174 (2015).
377 [6] Y. Shiota, T. Nozaki, F. Bonell, S. Murakami, T. Shinjo, and Y. Suzuki, Nat. Mater. **11**,
378 39 (2012).
379 [7] S. Kanai, M. Yamanouchi, S. Ikeda, Y. Nakatani, F. Matsukura, and H. Ohno, Appl. Phys.
380 Lett. **101**, 122403 (2012).
381 [8] C.-G. Duan, J.P. Velev, R.F. Sabirianov, Z. Zhu, J. Chu, S.S. Jaswal, and E.Y. Tsymbal,
382 Phys. Rev. Lett. **101**, 137201 (2008).
383 [9] K. Nakamura, R. Shimabukuro, Y. Fujiwara, T. Akiyama, T. Ito, and A.J. Freeman, Phys.
384 Rev. Lett. **102**, 187201 (2009).
385 [10] M. Tsujikawa and T. Oda, Phys. Rev. Lett. **102**, 247203 (2009).
386 [11] S.E. Barnes, J. Ieda, and S. Maekawa, Sci. Rep. **4**, 4105 (2014).
387 [12] S. Miwa, M. Suzuki, M. Tsujikawa, K. Matsuda, T. Nozaki, K. Tanaka, T. Tsukahara, K.
388 Nawaoka, M. Goto, Y. Kotani, T. Ohkubo, F. Bonell, E. Tamura, K. Hono, T. Nakamura,
389 M. Shirai, S. Yuasa, and Y. Suzuki, Nat. Commun. **8**, 15848 (2017).
390 [13] K. Nakamura, T. Nomura, A.-M. Pradipto, K. Nawa, T. Akiyama, and T. Ito, J. Magn.
391 Magn. Mater. **429**, 214 (2017).
392 [14] T. Nozaki, A. Kozioł-Rachwał, M. Tsujikawa, Y. Shiota, X. Xu, T. Ohkubo, T. Tsukahara,
393 S. Miwa, M. Suzuki, S. Tamaru, H. Kubota, A. Fukushima, K. Hono, M. Shirai, Y. Suzuki,
394 and S. Yuasa, NPG Asia Mater. **9**, e451 (2017).
395 [15] T. Nozaki, M. Endo, M. Tsujikawa, T. Yamamoto, T. Nozaki, M. Konoto, H. Ohmori, Y.
396 Higo, H. Kubota, A. Fukushima, M. Hosomi, M. Shirai, Y. Suzuki, and S. Yuasa, APL Mater.
397 **8**, 011108 (2020).
398 [16] H. Nakayama, T. Nozaki, T. Nozaki, and S. Yuasa, Appl. Phys. Lett. **122**, 032403 (2023).
399 [17] H. Nakayama, T. Nozaki, T. Nozaki, and S. Yuasa, Adv. Mater. Interfaces **10**, 2300131
400 (2023).

ACCEPTED MANUSCRIPT
APL Materials
AIP Publishing
This is the author's peer reviewed, accepted manuscript. However, the online version of record will be different from this version once it has been copyedited and typeset.
PLEASE CITE THIS ARTICLE AS DOI: 10.1063/5.0224193
13 November 2024 11:19:34

[18] T. Hirai, T. Koyama, and D. Chiba, Appl. Phys. Lett. **112**, 122408 (2018).

[19] T. Nozaki, S. Tamaru, M. Konoto, T. Nozaki, H. Kubota, A. Fukushima, and S. Yuasa, Sci. Rep. **11**, 21448 (2021).

[20] T. Nozaki, J. Okabayashi, T. Nozaki, and S. Yuasa, Sci. Rep. **13**, 10640 (2023).

[21] D. Chiba, S. Fukami, K. Shimamura, N. Ishiwata, K. Kobayashi, and T. Ono, Nat. Mater. **10**, 853 (2011).

[22] Y. Shiota, F. Bonell, S. Miwa, N. Mizuochi, T. Shinjo, and Y. Suzuki, Appl. Phys. Lett. **103**, 082410 (2013).

[23] T. Koyama, A. Obinata, Y. Hibino, and D. Chiba, Appl. Phys. Express **6**, 123001 (2013).

[24] T. Nozaki, T. Nozaki, H. Onoda, H. Nakayama, T. Ichinose, T. Yamamoto, M. Konoto, and S. Yuasa, APL Mater. **10**, 081103 (2022).

[25] J. Shiogai, T. Ohashi, T. Yang, M. Kohda, T. Seki, K. Takanashi, and J. Nitta, J. Phys. D.: Appl. Phys. **49**, 03LT01 (2015).

[26] Y. Hibino, T. Hirai, K. Hasegawa, T. Koyama, and D. Chiba, Appl. Phys. Lett. **111**, 132404 (2017).

[27] T. Maruyama, Y. Shiota, T. Nozaki, K. Ohta, N. Toda, M. Mizuguchi, A.A. Tulapurkar, T. Shinjo, M. Shiraishi, S. Mizukami, Y. Ando, and Y. Suzuki, Nat. Nanotechnol. **4**, 158 (2009).

[28] K. Nakamura, T. Akiyama, T. Ito, M. Weinert, and A.J. Freeman, Phys. Rev. B **81**, 22409(R) (2010).

[29] T. Hirai, T. Koyama, and D. Chiba, Phys. Rev. B **101**, 014447 (2020).

[30] P.H. Lin, B.Y. Yang, M.H. Tsai, P.C. Chen, K.F. Huang, H.H. Lin, and C.H. Lai, Nat. Mater. **18**, 335 (2019).

[31] S. Peng, D. Zhu, W. Li, H. Wu, A.J. Grutter, D.A. Gilbert, J. Lu, D. Xiong, W. Cai, P. Shafer, K.L. Wang, and W. Zhao, Nat. Electron. **3**, 757 (2020).

[32] B. Fang, L. Sánchez-Tejerina San José, A. Chen, Y. Li, D. Zheng, Y. Ma, H. Algaidi, K. Liu, G. Finocchio, and X. Zhang, Adv. Funct. Mater. **32**, 2112406 (2022).

ACCEPTED MANUSCRIPT
APL Materials
AIP Publishing
This is the author's peer reviewed, accepted manuscript. However, the online version of record will be different from this version once it has been copyedited and typeset.
PLEASE CITE THIS ARTICLE AS DOI: 10.1063/5.0241?3
13 November 2024 11:19:34

AIP Publishing APL Materials ACCEPTED MANUSCRIPT

This is the author's peer reviewed, accepted manuscript. However, the online version of record will be different from this version once it has been copyedited and typeset.
PLEASE CITE THIS ARTICLE AS DOI: 10.1063/5.0224193

13 November 2024 11:19:34

Figures

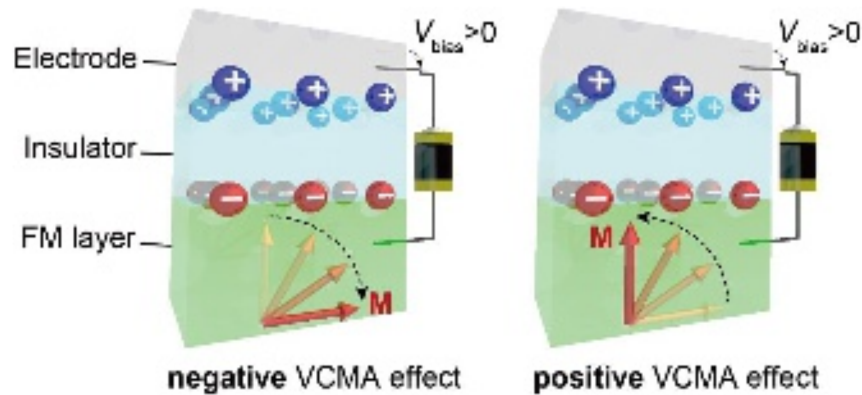

FIG. 1. Schematic illustration of the negative and positive voltage-controlled magnetic anisotropy (VCMA) effect in ferromagnetic metal (FM)/insulator/electrode stacked structures, where **M** and V_{bias} are the magnetization vector of ferromagnetic layer and the applied bias voltage, respectively. The positive bias voltage drives electron accumulation at the FM/insulator interface. For the junction with the negative (positive) VCMA effect, the perpendicular magnetic anisotropy (PMA) decreases (increases) with applying a positive bias voltage.

ACCEPTED MANUSCRIPT
APL Materials
AIP Publishing
This is the author's peer reviewed, accepted manuscript. However, the online version of record will be different from this version once it has been copyedited and typeset.
PLEASE CITE THIS ARTICLE AS DOI: 10.1063/5.0224193
13 November 2024 11:19:34

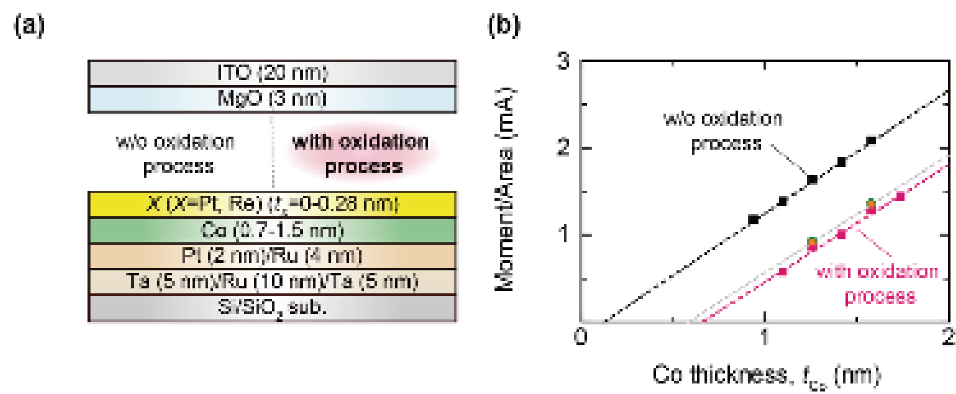

FIG. 2. Influence of the post-oxidization on the magnetic properties of Co/MgO junctions. (a) Schematic of the multilayer film without and with oxidation process. A layer of heavy metal X (=Pt or Re) is inserted between the Co layer and the MgO barrier. (b) Co layer thickness t_{Co} dependence of the saturation magnetic moment per unit area for Co/MgO multilayer with and without oxidation process. The orange and green plots are the data with insertion of Pt and Re with the thickness of 0.03 nm, respectively.

AIP Publishing
APL Materials
ACCEPTED MANUSCRIPT
This is the author's peer reviewed, accepted manuscript. However, the online version of record will be different from this version once it has been copyedited and typeset.
PLEASE CITE THIS ARTICLE AS DOI: 10.1063/5.0224193

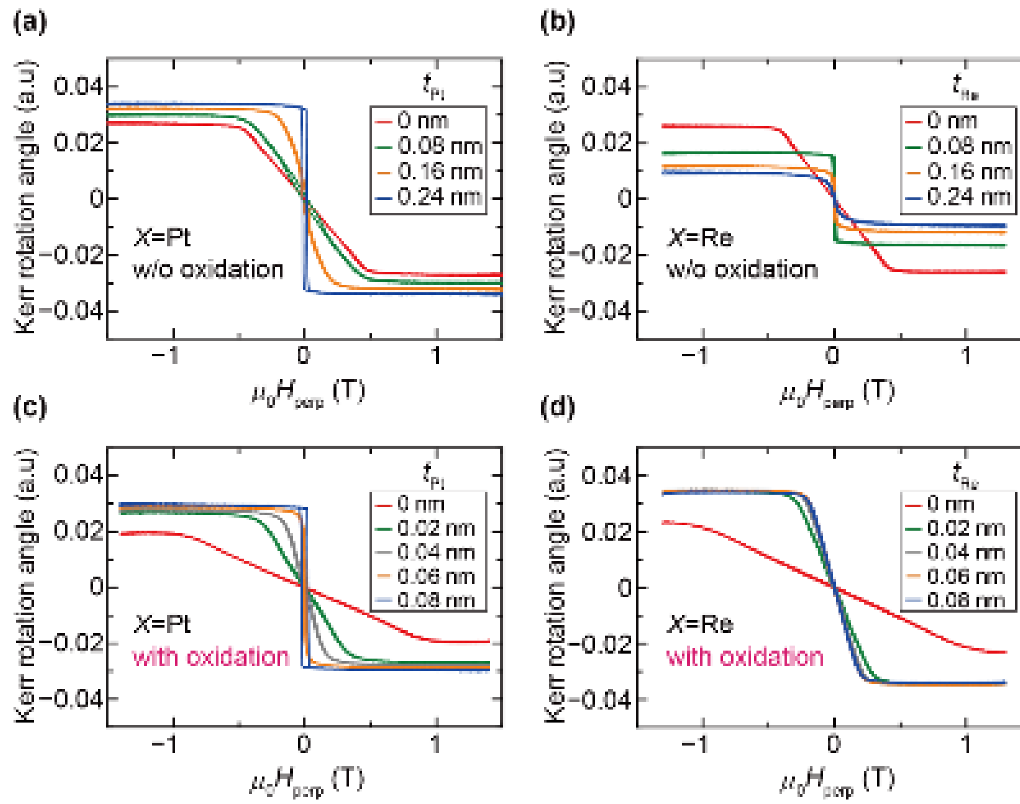

FIG. 3. Polar-MOKE measurements on interface engineered Co/*X*/MgO multilayer films. (a),(b) Polar-MOKE hysteresis curves for Co/*X*/MgO without an oxidation process with different thicknesses of inserted (a) Pt and (b) Re layers. (c),(d) Polar-MOKE hysteresis curves for Co/*X*/MgO with the oxidation process with different thicknesses of inserted (c) Pt and (d) Re layers. Here, the effective thickness of Co t_{Co}* is fixed at 0.8 nm. The polar MOKE measurements were conducted by applying a magnetic field perpendicular to the film plane.

13 November 2024 11:19:34

ACCEPTED MANUSCRIPT
APL Materials
AIP Publishing
This is the author's peer reviewed, accepted manuscript. However, the online version of record will be different from this version once it has been copyedited and typeset.
PLEASE CITE THIS ARTICLE AS DOI: 10.1063/5.0224193
13 November 2024 11:19:34

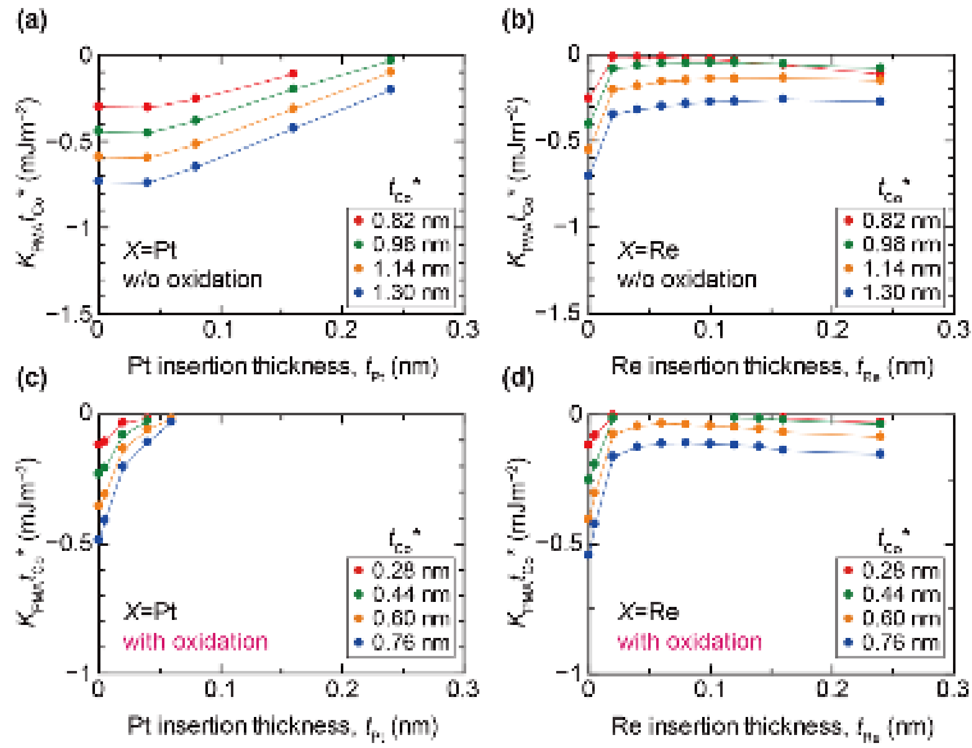

FIG. 4. Perpendicular magnetic anisotropy energies of Co/*X*/MgO multilayer films without and with oxidation process. (a),(b) *X* thickness dependence of $K_{PMA}t_{Co}$* for multilayer films with (a) Pt and (b) Re layers without oxidation process. (c),(d) *X* thickness dependence of $K_{PMA}t_{Co}$* for multilayer films with (c) Pt and (d) Re layers with the oxidation process.

AIP Publishing
APL Materials
ACCEPTED MANUSCRIPT
This is the author's peer reviewed, accepted manuscript. However, the online version of record will be different from this version once it has been copyedited and typeset.
PLEASE CITE THIS ARTICLE AS DOI: 10.1063/5.0224193

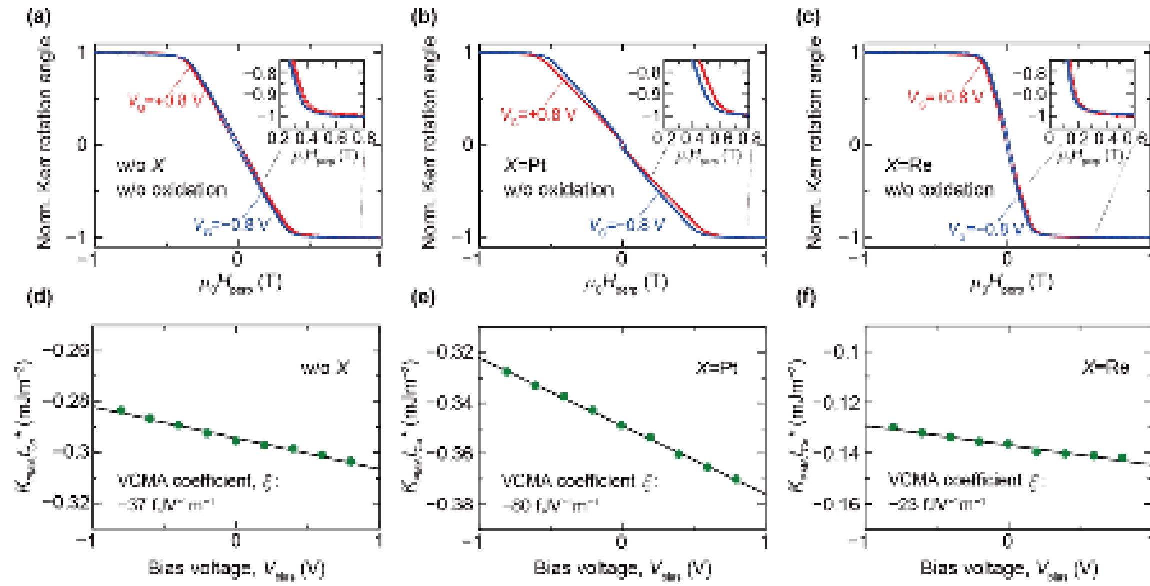

FIG. 5. Magnetoelectric properties of Co/MgO and Co/*X*/MgO multilayer devices without oxidation process. (a)-(c) Normalized polar-MOKE hysteresis curves of multilayer devices with (a) Co/MgO, (b) Co/Pt/MgO, and (c) Co/Re/MgO junctions, where the effective thickness of Co is fixed at 0.8 nm. (d)-(f) Bias voltage dependence of $K_{PMA}t_{Co}$* obtained for multilayer devices with (d) Co/MgO, (e) Co/Pt/MgO, and (f) Co/Re/MgO junctions. The solid lines are linear fits to the data.

13 November 2024 11:19:34

ACCEPTED MANUSCRIPT
APL Materials
AIP Publishing
This is the author's peer reviewed, accepted manuscript. However, the online version of record will be different from this version once it has been copyedited and typeset.
PLEASE CITE THIS ARTICLE AS DOI: 10.1063/5.0224193
13 November 2024 11:19:34

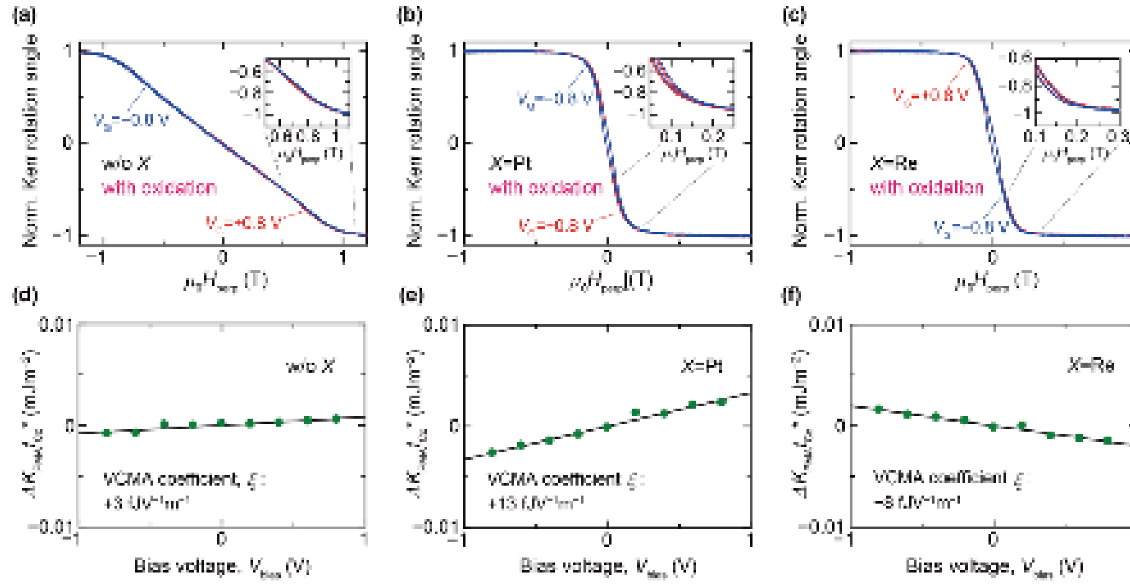

FIG. 6. Magnetoelectric properties of Co/MgO and Co/X/MgO multilayer devices with an oxidation process. (a)-(c) Normalized polar-MOKE hysteresis curves of multilayer devices with (a) Co/MgO, (b) Co/Pt/MgO, and (c) Co/Re/MgO junctions, where the effective thickness of Co is fixed at 0.8 nm. (d)-(f) Change of $\Delta K_{PMA}t_{Co}$* due to bias voltage for multilayer devices with (d) Co/MgO, (e) Co/Pt/MgO, and (f) Co/Re/MgO junctions. The solid lines are linear fits to the data.

ACCEPTED MANUSCRIPT
APL Materials
AIP Publishing
This is the author's peer reviewed, accepted manuscript. However, the online version of record will be different from this version once it has been copyedited and typeset.
PLEASE CITE THIS ARTICLE AS DOI: 10.1063/5.0224193

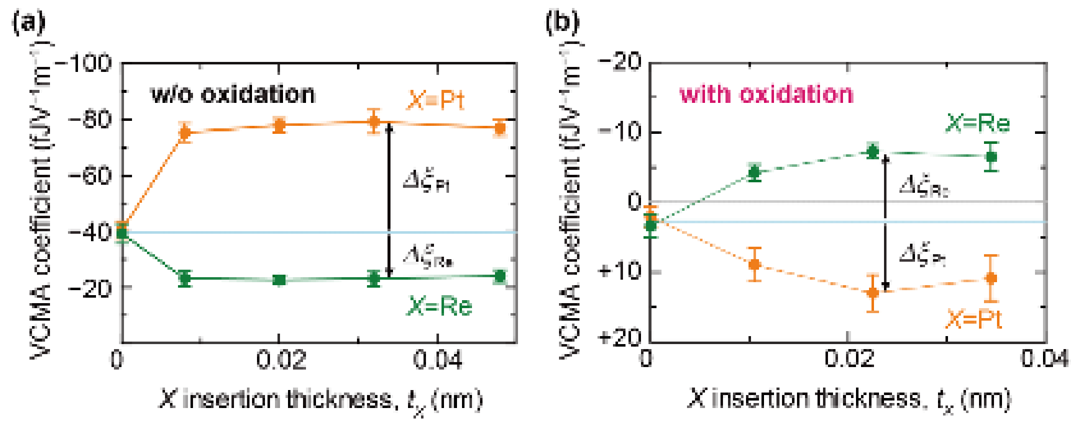

FIG. 7. X layer thickness t_X dependence of VCMA coefficient. (a),(b) VCMA coefficient plotted as a function of t_X for Co/X/MgO multilayer films (a) without and (b) with oxidation process. $\Delta\xi$ corresponds to the additional VCMA effect induced by the insertion of heavy metal X layers. Here, we have placed the negative values at the top of the vertical axis since the sign of the VCMA effect in most materials is negative.

13 November 2024 11:19:34